Available online at www.sciencedirect.com

SciVerse ScienceDirect

Acta Materialia 60 (2012) 6175–6182

Acta MATERIALIA

www.elsevier.com/locate/actamat

Electronic band structures, dielectric functions and interband transitions of relaxor ferroelectric (1-x) Pb ($Sc_{1/2}Ta_{1/2}$) O_3-$x$$PbHfO_3$ ceramics: A spectroscopic reflectance study

W.J. Zhang [a], Z.H. Duan [a], K. Jiang [a], Z.G. Hu [a,*], G.S. Wang [b], X.L. Dong [b], J.H. Chu [a]

[a] *Key Laboratory of Polar Materials and Devices, Ministry of Education, Department of Electronic Engineering, East China Normal University, Shanghai 200241, People's Republic of China*

[b] *Key Laboratory of Inorganic Functional Materials and Devices, Shanghai Institute of Ceramics, Chinese Academy of Sciences, Shanghai 200050, People's Republic of China*

Received 18 January 2012; received in revised form 29 July 2012; accepted 29 July 2012
Available online 24 August 2012

Abstract

Electronic band structures and dielectric functions of relaxor ferroelectric (1-x) Pb ($Sc_{1/2}Ta_{1/2}$) O_3-$x$$PbHfO_3$ (PSTH) ceramics ($0 \leqslant x \leqslant 0.2$) have been investigated by far-IR–UV reflectance spectra. Based on generalized four-parameter damped oscillators and Tauc–Lorentz dispersion models, the dielectric functions from 0.006 to 6 eV have been successfully extracted at room temperature. The status of structural order can be characterized by combining the strength of the Sc–Ta vibrational mode and the dielectric loss in the frequency range of 280–320 cm^{-1}. It was found that the electronic structures (which depend closely on the BO_6 (B = Sc, Ta Hf) octahedron) are sensitive to the B-site atom concentration. The interband transitions can be clearly demonstrated by the imaginary part of the dielectric function which corresponds to the transition from the O 2p to B-site (Sc, Ta and Hf) d states and Pb 6p states. The two typical transition energies show the opposite trend with increased $PbHfO_3$ composition. Remarkable variations of the B-site order degree and the lattice expansion due to the introduction of $PbHfO_3$ are responsible for modifications of the dielectric function and electronic structures. These results could be crucial for investigating the potential applications of PSTH-based optoelectronic and pyroelectric devices.

Keywords: Relaxor ferroelectric; Electronic structure; Dielectric function; (1-x) Pb ($Sc_{1/2}Ta_{1/2}$) O_3-$x$$PbHfO_3$

1. Introduction

Perovskite ferroelectrics have attracted considerable attention due to a wide range of applications, such as multilayered ceramic capacitors, high-strain actuators, high-density information storage, high-speed processing as well as for telecommunications and military applications [1–3]. Among these materials, lead-based ferroelectrics such as $PbMg_{1/3}Nb_{2/3}O_3$ (PMN), $PbZn_{1/3}Nb_{2/3}O_3$ (PZN), $PbSc_{1/2}Nb_{1/2}O_3$ (PSN) and $PbSc_{1/2}Ta_{1/2}O_3$ (PST) are typical relaxor ferroelectrics. All these compounds show high dielectric permittivity, strong electrostrictive, excellent pyroelectric and electro-optic coefficients [2–4]. The pyroelectric effect of ferroelectric materials can be used for uncooled thermal imaging, IR detection, radiation and pyroelectric sensors [2,5]. In particular, PST is a well-known relaxor ferroelectric with a complex perovskite structure of $AB'B''O_3$, where A sites are occupied by Pb^{2+} and B sites are shared by Sc^{3+} and Ta^{5+} ions. Sc^{3+} and Ta^{5+} cations may occupy B sites randomly or can develop 1:1 NaCl-type order on the {111} planes. PST material is of special interest because the ordering degree of B site ions can be controlled by thermal treatment and/or other growth parameters. The order degree depends upon the difference in the valence states and the size of two B-site ions [5,6]. As is known, ordered PST is a normal ferroelectric with a spontaneous ferroelectric phase transition around 300 K, while

* Corresponding author. Tel.: +86 21 54345150; fax: +86 21 54345119.
E-mail address: zghu@ee.ecnu.edu.cn (Z.G. Hu).

1359-6454/$36.00
http://dx.doi.org/10.1016/j.actamat.2012.07.061

disordered PST seems to be a relaxor with a phase transition around 270 K [4]. Generally, electrical and optical responses will show different behaviors for PST with the order degree because the electronic structures are expected to show a slight discrepancy. Although it was reported that the B-site order has a dramatic effect on the dielectric response and the peak permittivity [6,7], few studies on optical properties for PST and relative materials have been presented to date.

On the other hand, dielectric and pyroelectric studies of solid solutions for relaxor ferroelectric PST with normal ferroelectrics such as $PbTiO_3$ and $PbZrO_3$ revealed many dielectric and pyroelectric properties [8–10]. Furthermore, mixing ferroelectrics with $PbHfO_3$ can increase the Curie temperature of PST ceramics, decrease the sintering temperature and tailor the structural ordering. Liu et al. also found that Pb $(Sc_{1/2}Ta_{1/2})$ O_3-$PbHfO_3$ (PSTH) ceramics showed enhanced dielectric and pyroelectric properties [11]. The literature contains reports on the IR dielectric function, electronic band structures, ferroelectric properties and influences from the A or B site on the structure for lead-based relaxor ferroelectrics [1,4,6,12]. Recently, the lattice vibration and phase transition properties of PSTH ceramics have been examined using temperature-dependent Raman spectra [13]. Unfortunately, no further studies on the optical properties of PSTH ceramics in a wider phonon energy region (especially for optical functions and higher-energy interband transitions) have been reported to date. The optical function plays an important role in the optoelectronic device design. Furthermore, the dielectric function (which can be directly related to the electronic band structures of materials) not only provides optical properties, but also is critical for developing optical electronics devices. Fortunately, reflectance spectroscopy can present some invaluable information on the phonon mode behaviors, order–disorder phenomena, dielectric function of materials and electronic band energy. Therefore, it is desirable to carry out a detailed study on PSTH material regarding these essential properties.

In this article, optical properties and higher-energy interband transitions of ordered and disordered PSTH ceramics have been studied in the far-IR–UV photon energy range. Effects from the $PbHfO_3$ addition on electronic band structures are discussed in detail.

2. Experimental details

PSTH nanocrystalline powders ($x = 0.00$, 0.05, 0.10, 0.15 and 0.20) were first synthesized by the two-stage calcination route. Raw materials Sc_2O_3 (99.99%), Ta_2O_5 (99.99%) and HfO_2 (99.99%) were weighed according to their stoichiometry and mixed by ball milling for 24 h. The mixture was dried, sieved and pressed under a pressure of 10 MPa. Then the samples were placed in an alumina crucible, batched and calcined at 1350 °C for 4 h to form a HfO_2-modified $ScTaO_4$ phase. The milled powders were then calcined with PbO (99.99%) at 1150 °C for 2 h, and the PSTH ceramics were prepared by the hot-pressing sintering method. Samples with 5 wt.% excess PbO (99.99%) were first heated to 900 °C and then heated to 1320 °C under an oxygen pressure of 25 MPa for 2 h. Finally, the samples were obtained by cooling to 900 °C at a rate of 3 °C min^{-1}. All ceramic wafers were double-side polished for spectral measurements. Details regarding the preparation of the ceramics can be found in Refs. [10,11].

The crystalline structure of PSTH ceramics was analyzed by X-ray diffraction (XRD) using Cu $K\alpha$ radiation (Rigaku D/MAX-2550 V, Tokyo, Japan). Samples are found to be well crystallized in the single phase. There are no detectable secondary phases, which indicates the complete solid solution of the PST and $PbHfO_3$ compositions. The XRD pattern shows that the perovskite structure contains no impurity phases [11]. XRD spectra of PSTH ceramics in the range of 17°-25° are shown in the inset of Fig. 1. The superlattice reflection (111) peak and (200) diffraction peaks are marked. The intensity of peak (111) decreases with increased composition and almost disappears for PSTH ceramics ($x = 0.1$, 0.15, and 0.2). Based on the two peaks, the degree of structural ordering can be evaluated. By increasing the $PbHfO_3$ composition, the degree of structural ordering is calculated to be 0.72, 0.42, 0, 0 and 0, respectively, which indicates that the B-site ordering decreases and the ceramics become completely disordered by increasing the $PbHfO_3$ composition.

Near-normal incident reflectance spectra (about 8°) were recorded by a double-beam UV–IR spectrophotometer

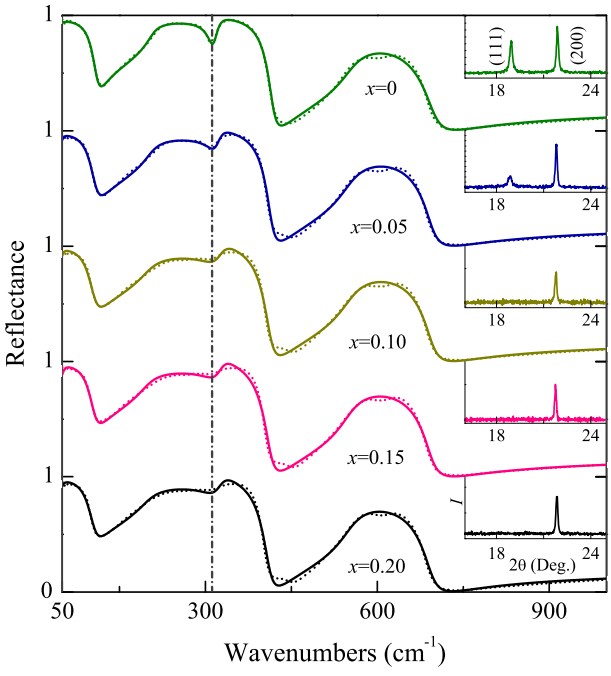

Fig. 1. Experimental IR reflectance spectra (dotted lines) and best-fit results (solid lines) of (1-x) $PbSc_{1/2}Ta_{1/2}O_3$-$x$$PbHfO_3$ ceramics. Each spectrum is successively shifted by 1.0 in the vertical direction. Note that the dashed line indicates the variation trend from the lattice vibrations. The XRD spectra in the range of 17°-25° from PSTH ceramics are plotted in the insets and the diffraction peaks (111) and (200) are marked.

(PerkinElmer UV/VIS Lambda 950) at photon energies of 2255–208 nm (0.55–6.0 eV) with a spectral resolution of 1 nm. An aluminum (Al) mirror, whose absolute reflectance was directly measured, was taken as the reference for spectra in the photon energy region. Near-normal incident IR reflectance measurements were performed over the frequency from 50 to 8000 cm^{-1} (0.006–0.992 eV) using a Fourier transform infrared (FTIR) spectrometer (Bruker Vertex 80 V). The spectral resolution was 2 cm^{-1} and 4 cm^{-1} in the low- and high-frequency ranges, respectively. Different beamsplitters of optimized KBr or 6-μm thick mylar were used with a liquid nitrogen cooled mercury cadmium telluride (MCT) or room temperature deuterated triglycine sulfate (DTGS) detector for each IR region. Gold and aluminum mirrors whose absolute reflectance was measured were taken as references for spectra in the high- and low-frequency regions. Note that the samples were at room temperature for all measurements and no mathematical smoothing has been performed for the experimental data.

3. Results and discussion

3.1. FTIR reflectance spectra

Although the real and imaginary part of the dielectric function can be obtained by Kramers–Krönig analysis in the experimental frequency range, the analysis depending on the extrapolation procedure of reflectivity out of the measured spectra range would be inaccurate because the corresponding approximation must be applied [14,15]. Nevertheless, a fitting method with suitable dispersion model is frequently applied to extract the dielectric function of studied materials. Note that there are many dielectric function models which correspond to different physical processes existing in the material system. Therefore, IR reflectance spectra of PSTH ceramics were fitted by using the generalized four-parameter damped oscillator model with the factorized form of the complex dielectric function:

$$\tilde{\varepsilon}(\omega) = \varepsilon_{\infty,\mathrm{IR}} \prod_{i=1}^{n} \frac{\omega_{Li}^2 - \omega^2 + i\omega\gamma_{Li}}{\omega_{Ti}^2 - \omega^2 + i\omega\gamma_{Ti}}. \quad (1)$$

where $\tilde{\varepsilon}(\omega)$ is related to reflectivity $R(\omega)$ by:

$$R(\omega) = \left| \frac{\sqrt{\tilde{\varepsilon}(\omega)} - 1}{\sqrt{\tilde{\varepsilon}(\omega)} + 1} \right|^2. \quad (2)$$

Here, $\varepsilon_{\infty,\mathrm{IR}}$ is the dielectric constant caused by electronic polarization at a higher frequency, ω_{Ti}, ω_{Li}, γ_{Ti} and γ_{Li} represent, respectively, the transverse and longitudinal eigenfrequencies of the ith polar mode and their respective damping constants [6,14,16]. The generalized four-parameter oscillator model was used to achieve a good fit with minimum numbers of physically meaningful oscillators. IR reflectance can provide information about lattice vibrations, the position of the ions and also can be a sensitive tool to detect the B-site ordering degree. Experimental and fitting IR reflectance spectra of all five PSTH ceramics in the frequency range 50–1000 cm^{-1} (0.006–0.992 eV) are shown in Fig. 1. The spectra range above 1000 cm^{-1} is not shown because the reflectivity is almost flat and there is no phonon response in the frequency region. Short dashed lines are experimental data, and solid lines are fitting results with the four-parameter damped oscillator model. There is a good fit throughout the measured frequency region. One can see that all spectra show similar behavior, which corresponds to the $PbHfO_3$ composition because the small doping composition only slightly influences the phonon intensity, broadening and frequency. However, there is a distinct variation in the frequency region of 280–320 cm^{-1} which is sensitive to the ordered structure as shown by the dashed line in Fig. 1. Phenomena are similar to IR data from PST ceramics [6]. The best parameters of the four-parameter damped oscillator model are listed in Table 1.

According to group theory, there are three IR active modes for the disordered perovskite structure ($Pm\bar{3}m$) and four modes for the ordered phase ($Fm\bar{3}m$) in the paraelectric phase. However, there are at least 16 and 7 IR modes in the ferroelectric phase for the ordered and disordered samples, respectively [17], which means that additional modes in the ferroelectric phase should appear by splitting of both IR and Raman active modes. Note that four IR active modes can be observed in the present spectra. For ordered PSTH ($x = 0$, 0.05) ceramics with a paraelectric phase, observed IR modes agree with predicted modes. However, for disordered PSTH ($x = 0.10$, 0.15 and 0.20) ceramics which are located in the ferroelectric phase, differences between numbers of observed and theoretically modes can be explained by the fact that the predicted mode splitting is too small to be distinguished. The phonon splitting in the rhombohedral phase cannot be observed, which may be due to the high damping; it is also smaller than the soft mode splitting in simple perovskite ferroelectrics [18]. IR spectra can be divided into three characteristic frequency regions: (1) Pb–BO_6 stretching modes below 150 cm^{-1}; (2) mixed B–O–B bending and O–B–O stretching modes in the frequency region 150–500 cm^{-1}; and (3) B–O–B stretching modes at 500–900 cm^{-1}. The frequency band near 60 cm^{-1} corresponds to Pb–O_6 octahedra external translations (Last mode). The mode near 210 cm^{-1} is predominantly assigned to the B–O_6 stretching mode (Slater mode). The highest phonon frequency near 550 cm^{-1} is related to Sc/Ta–O_6 octahedral bending (Axe mode). The third vibration located at 318 cm^{-1} corresponds to the Sc–Ta stretching mode which has F_{1u} symmetry due to the B-site local ordering [17,19]. A similar mode at 330 cm^{-1} can also be seen in IR spectra of a PMN single crystal with B-site short-range ordering [20–22]. Nevertheless, the phonon mode is forbidden for the disordered samples. On the other hand, the assignment of the modes for the PSTH material by nature is difficult because the system is heterogeneous. Note that the phonon modes can be affected by the depolarization, lattice defects and can be

Table 1
Four-parameter damped oscillator model parameter values for PSTH ceramics are extracted from the best fitting far-IR reflectance spectra in Fig. 1; the 90% reliability of the fitting parameters is given in parentheses.

Samples	$\varepsilon_{\infty,IR}$	F_{1u}				F_{1u}				F_{1u}				F_{1u}			
x		ω_{L1} (cm^{-1})	γ_{L1} (cm^{-1})	ω_{T1} (cm^{-1})	γ_{T1} (cm^{-1})	ω_{L2} (cm^{-1})	γ_{L2} (cm^{-1})	ω_{T2} (cm^{-1})	γ_{T2} (cm^{-1})	ω_{L3} (cm^{-1})	γ_{L3} (cm^{-1})	ω_{T3} (cm^{-1})	γ_{T3} (cm^{-1})	ω_{L4} (cm^{-1})	γ_{L4} (cm^{-1})	ω_{T4} (cm^{-1})	γ_{T4} (cm^{-1})
0	6.48	111	20.8	45	9.1	314	21.1	207	21.9	418	19.1	318	15.7	699	36.6	554	50.9
	(0.03)	(0.91)	(1.94)	(9.16)	(2.67)	(1.86)	(3.95)	(1.79)	(2.6)	(1.58)	(1.67)	(1.58)	(3.22)	(1.53)	(3.74)	(1.81)	(3.08)
0.5	6.14	109	26.7	51	4.9	320	29.6	206	30.2	416	20.6	321	21.9	695	9.5	551	49.3
	(0.02)	(1.09)	(2.20)	(3.63)	(2.43)	(3.54)	(7.46)	(1.80)	(2.95)	(0.71)	(1.83)	(2.86)	(5.99)	(1.50)	(3.18)	(1.78)	(2.98)
0.1	6.21	107	29.1	51	4.1	325	44.1	202	40.1	414	23.7	325	33.1	695	29.9	552	49.5
	(0.03)	(1.23)	(2.53)	(3.13)	(2.51)	(5.75)	(11.73)	(2.09)	(3.64)	(0.79)	(2.17)	(4.58)	(9.23)	(1.54)	(3.37)	(1.86)	(3.09)
0.15	6.02	107	27.1	52	5.6	325	39.6	199	38.1	414	24.2	325	29.6	694	29.6	551	47.1
	(0.03)	(1.41)	(2.89)	(3.33)	(3.14)	(6.17)	(12.5)	(2.45)	(4.13)	(0.97)	(2.65)	(4.96)	(9.97)	(1.86)	(3.96)	(2.17)	(3.59)
0.2	6.47	107	29.1	51	5.6	324	41.5	200	41.6	412	23.6	324	31.3	694	31.3	552	47.1
	(0.03)	(1.46)	(2.89)	(4.49)	(3.12)	(6.31)	(12.8)	(2.47)	(4.14)	(0.89)	(2.45)	(5.06)	(10.15)	(1.70)	(3.90)	(2.04)	(3.39)

identified as geometrical modes [23]. However, the present assignment appears reasonable since results are derived from the combination of Raman scattering, IR spectra and XRD measurements [13].

3.2. Lattice vibrations

The fitted parameter values and the relation between the phonon frequency and $PbHfO_3$ compositions are displayed in Fig. 2. Compared with phonon mode behavior investigated by Raman scattering, two low-frequency F_{1u} phonon modes were observed due to different selection rules [13]. The four transverse-optical (TO) modes can be sufficiently expressed by $(47.6 + 25.4x)$, $(207–42.0x)$, $(319 + 32.9x)$ and $(553–8.4x)$ cm^{-1}, respectively, which suggests that IR phonon frequencies are slightly perturbed by the Hf ion introduction. The phonon frequency of the TO_1 mode in ordered samples is lower than the TO_1 mode in disordered samples. This mode shows a blue-shift pattern due to the stretch of the Pb–O–Ta bonds average length which is caused by $PbHfO_3$ incorporation. The TO_2 mode frequency is 207 and 200 cm^{-1} for pure PST and PSTH ($x = 0.20$) ceramics, respectively which suggests that the phonon frequency shifts towards the lower-frequency side. On the other hand, damping constants of the TO_2 mode for ordered samples are smaller than constants for disordered samples. Fig. 1 confirms that the TO_2 mode broadens in disordered PSTH ceramics. This phenomena may be ascribed to the B-site effect ordering on the B–O_6 stretching. The TO_3 mode near 318 cm^{-1} should be activated only in ordered or partially ordered samples. Dielectric strengths of the TO_3 phonon mode were used to estimate the B-site degree which was calculated using the formula [17]:

$$\Delta\varepsilon_3 = \frac{\varepsilon_{\infty,IR}}{\omega_{T3}^2} \frac{\prod_j \left(\omega_{Lj}^2 - \omega_{T3}^2\right)}{\prod_{j\neq 3} \left(\omega_{Tj}^2 - \omega_{T3}^2\right)}. \quad (3)$$

The PSTH ($x = 0$,0.05) strength is 0.35, 0.07 and the PSTH ($x = 0.1$, 0.15 and 0.2) strength is 0, which indicates that the B-site degree decreases with increased $PbHfO_3$ composition and becomes completely disordered. It also suggests that the TO_3 mode is much weaker and broader in disordered ceramics. It should be noted that results are consistent with data from XRD spectra shown in the insets of Fig. 1. These phenomena are also supported by Raman scattering [13]. The TO_3 phonon mode shifts towards higher wavenumbers due to the substitution of Hf atoms which decreases the reduced mass of Sc and Ta atoms. As can be seen, the TO_4 phonon mode also slightly decreases with $PbHfO_3$ composition, which means that the B-site order can be affected by the Hf incorporation and further influences the Sc/Ta-O_6 and Sc–Ta stretching mode. On the other hand, corresponding longitudinal-optical (LO) phonon modes can be expressed by $(111–22.9x)$, $(316 + 54.8x)$, $(418–29.1x)$ and $(698–21.8x)$ cm^{-1}, respectively. The positions of four LO vibrations change with $PbHfO_3$ composition. The maximal difference of the second LO phonon mode is about 10 cm^{-1}. The crystalline disorder (e.g. chemical composition perturbation) is sensi-

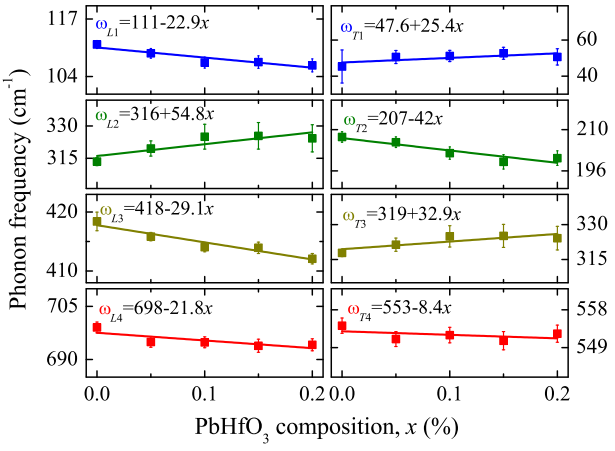

Fig. 2. The $PbHfO_3$ composition dependence of the longitudinal and transverse optical phonon mode (F_{1u}) frequencies in the left and right panel, respectively. Note that the solid lines are the linearly fitting results.

tive to ferroelectric transition [24,25]. In particular, the large splitting of the LO–TO phonon modes which is induced by the Coulomb interactions is strongly related to the dynamic polarization of lattice vibrations [24]. Note that PSTH ceramics have relatively large values of damping constants for high-frequency phonon modes which indicates a higher anharmonicity [26]. From this point of view, it can be concluded that the introduction of $PbHfO_3$ plays an important role in lattice vibrations which greatly modifies the polarization and phase transition properties of PSTH ceramics.

3.3. Ultraviolet–near-infrared spectral characteristics

To elucidate the higher photon energy region where the absorption appears to be due to the interband transition process for semiconductor/dielectric materials, it should be emphasized that the above generalized oscillator model is invalid at shorter wavelengths because it cannot explain the complicated behavior of many high-energy transitions (above the band-gap energy). To extract the dielectric function, the physical model expressing the band–band transitions must be applied. Moreover, the inverse synthesis method is based on a phenomenological model fitted to experimental results. The reliability of the inverse synthesis method depends mainly on the validity of the optical model and the fitting statistics. The Tauc–Lorentz (TL) model was constructed for each sample to obtain the optical properties of PSTH ceramics. The TL dispersion model is obtained from the Tauc joint density of states and the standard quantum mechanical or Lorentz calculation for ε_2 (imaginary part of the dielectric function) of a collection of noninteracting atoms, which can be written as:

$$\varepsilon_1(E) = \varepsilon_{\infty,\mathrm{UV}} + \frac{2}{\pi} P \int_{E_b}^{\infty} \frac{\xi \varepsilon_2(\xi)}{\xi^2 - E^2} d\xi,$$
$$\varepsilon_2(E) = \sum_{i=1}^{2} \frac{S_i E_{0i} \Gamma_i (E - E_{gi})^2}{\left(E^2 - E_{0i}^2\right)^2 + \Gamma_i^2 E^2} \frac{1}{E}. \quad (4)$$

where $\varepsilon_{\infty,\mathrm{UV}}$ is the high-frequency dielectric constant, P is the Cauchy principal part of the integral, E is the incident photon energy and S_i, E_{0i}, Γ_i and E_{gi} are the amplitude, peak position energy, broadening term and Tauc gap energy of the ith oscillator, respectively. The above TL model abides by the Kramers–Krönig transformation, which has been successfully applied to semiconductor and dielectric materials [27–29]. The fitting calculation on the reflectance is carried out by taking Eq. (2) into account, i.e. only considering the air–PSTH interface reflectance owing to the thickness of about 0.5 mm. It is noteworthy that both the four-parameter damped oscillator model and the TL model possess the complicated optical response behavior of the semiconductor and dielectric materials in wide photon energy regions. Moreover, one can expect that optical functions from the above Eqs. (1) and (4) are continuous within experimental errors in the overlapping region.

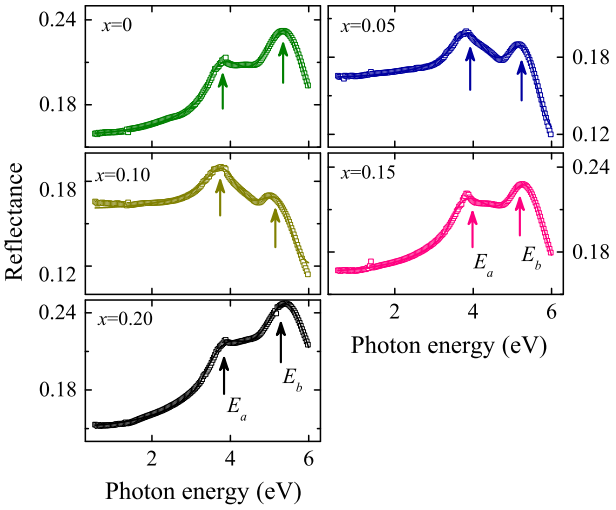

Fig. 3. Experimental (diamond) and the best-fit (solid lines) reflectance spectra of (1-x) $PbSc_{1/2}Ta_{1/2}O_3$-$x$$PbHfO_3$ ceramics from the UV to near-IR photon energy region. Arrows indicate the interband transitions corresponding to the critical point energy of E_a and E_b.

Experimental and best-fit reflectance spectra of PSTH ceramics at the incident angle of 8° from UV to the IR photon energy region are shown in Fig. 3. As can be seen, good agreement between the calculated and experimental spectra is obtained throughout the photon energy region. Based on the simulation, parameter values of the TL dielectric function model are summarized in Table 2. The main feature in Fig. 3 is a doublet structure caused by interband transitions (critical points, labeled as E_a and E_b), which is similar to perovskite phase compounds $PbZr_xTi_{1-x}O_3$ (PZT) and $KTa_{1/2}Nb_{1/2}O_3$ (KTN) [30,31]. Table 2 shows that the ratio S_1/S_2 increases with the composition ($x = 0$, 0.05 and 0.1), which means that the lower-energy transition is the dominant one and becomes more prominent with decreased degree of order. However, for disordered samples ($x = 0.1$, 0.15 and 0.2), the ratio decreases with increased composition of $PbHfO_3$, and the two transitions become comparable. In addition, $\Gamma_1 > \Gamma_2$ indicates that the broadening of the first oscillator is larger than that of the second oscillation (see Fig. 3), which suggests that the $PbHfO_3$ composition has a remarkable influence on interband transitions.

3.4. Optical functions from 0.006 to 6.0 eV

It is well known that the dielectric function plays an important role in the design, optimization and evaluation of optoelectronic devices. Fig. 4 shows the real and imaginary parts of the complex dielectric function from the four-parameter damped oscillator and TL models in the different photon energy regions, respectively. Note that optical constants in the transparent region can be well connected although different function models are applied. As can be seen, the dielectric response can be roughly divided into three distinct parts: (i) a lattice vibration component;

Table 2
Tauc–Lorentz parameter values for PSTH ceramics are determined from the simulation of near-IR–UV reflectance spectra in Fig.
3; the 90% reliability of the fitting parameters is given in parentheses.

$PbHfO_3$ composition x	$\varepsilon_{\infty,UV}$	E_a				E_b			
		S_1 (eV)	E_{01} (eV)	Γ_1 (eV)	E_{g1} (eV)	S_2 (eV)	E_{02} (eV)	Γ_2 (eV)	E_{g2} (eV)
0	3.90	165	3.35	1.51	3.39	72.3	5.39	1.28	4.27
	(0.03)	(46.8)	(0.18)	(0.13)	(0.02)	(3.78)	(0.01)	(0.04)	(0.05)
0.05	4.92	34.3	3.93	1.15	3.20	10.9	5.44	0.91	3.27
	(0.02)	(5.34)	(0.04)	(0.05)	(0.05)	(1.98)	(0.01)	(0.04)	(0.22)
0.10	4.95	17.3	3.94	1.08	2.95	2.38	5.44	1.03	1.25
	(0.02)	(3.81)	(0.04)	(0.07)	(0.10)	(0.72)	(0.02)	(0.07)	(0.65)
0.15	4.20	124	3.58	1.79	3.33	57.3	5.35	1.19	4.24
	(0.03)	(26.1)	(0.14)	(0.09)	(0.03)	(4.61)	(0.02)	(0.06)	(0.07)
0.20	3.38	84.4	3.90	1.93	3.21	79.5	5.35	1.43	4.11
	(0.06)	(17.7)	(0.07)	(0.24)	(0.03)	(8.41)	(0.02)	(0.08)	(0.15)

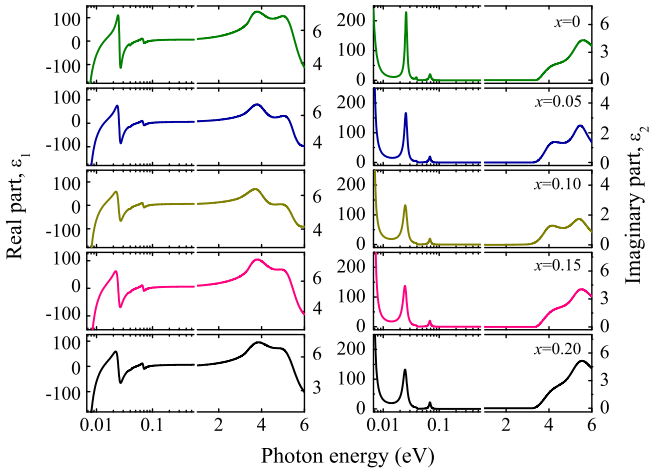

Fig. 4. Real and imaginary parts of the dielectric function in the photon energy of 0.006–6.0 eV for (1-x) $PbSc_{1/2}Ta_{1/2}O_3$-$x$$PbHfO_3$ ceramics. Different vertical coordinates in IR and UV regions are applied to enlarge the UV parts. To clarify, the horizontal coordinates in the IR region are logarithmic units. Note that optical constants in the transparent region can be sufficiently connected although different function models are applied.

(ii) a transparent oscillation; and (iii) an absorption in the high-frequency region. In the lattice vibration region, the dispersion is controlled by IR optical vibration modes and the peaks correspond to frequencies of phonon modes. There are some differences in peaks intensities which may be induced by the Hf^{4+} ion doping in the ordering and the lattice distortion of the Pb-based system. In the range of 280–320 cm^{-1}, PST ceramics (i.e. $x = 0$) have a maximal ε_2 and the ε_2 decreases with increased x, which indicates that the B-site degree is reduced. For disordered PSTH ($x = 0.1$, 0.15 and 0.2) ceramics, however, it remained almost kept unchanged.

The transparent region is limited in the high-energy region by the onset of absorption due to band-to-band electronic transitions and in the low-energy range by resonant bonding absorption. In this region, ε_1 continuously increases nonlinearly, whereas ε_2 is nearly constant (zero). The refractive index n at the photon energy 2 eV has been calculated by the formula: $n^2 - \kappa^2 = \varepsilon_1$; here κ is the extinction coefficient. The n value is about 2.375 for PSTH ($x = 0$) which is smaller than the n value of a PMN single crystal (2.522) and PZT films (2.54) [30,32]. As the $PbHfO_3$ composition increases, the refractive index of the PSTH ceramics decreases, a trend that is related to the variation in band gap, grain size and lattice expansion [32]. A sharp onset of the band-to-band absorption is observed for all samples and dominating features in this region are attributed to interband transitions. As can be seen, with increased $PbHfO_3$ composition, the intensity of ε_2 first decreases and then increases. This phenomenon is ascribed to the lattice expansion and/or the increase of oxygen vacancies with the introduction of $PbHfO_3$ [11]. For PSTH ($x = 0.2$) ceramics, the existence of Pb vacancies also affects the dielectric function. These results indicate that the introduction of $PbHfO_3$ or the variation of order parameters has an important effect on the dielectric responses in the high-frequency and low-frequency regions.

3.5. Electronic band structures

For simple ABO_3 perovskite-type compounds, the valance-band (VB) is primarily derived from oxygen 2p orbitals with bonding states of O and B-site atoms at the bottom of the VB and the oxygen non-bonding states at the VB maximum [33,34]. The conduction band (CB) minimum is made up mainly from the d t_{2g} of the B-site atom [33]. As is known, KTN, PZT, PMN and PST are typical $AB'B''O_3$ perovskite-type oxide materials, and hence electronic band structures of PSTH ceramics will be similar to structures of KTN, PZT and PMN. In the KTN, the VB mainly consists of O 2p states, whereas the p–d hybridization between most of the O 2p and Nb 4d together with Ta 5d orbitals also exists in the VB. Interband transitions are attributed to transitions from the O 2p VB to the Nb 4d or Ta 5d CB [31]. However, for Pb-based compounds, Pb–O bonding will affect the hybridization between O and B-site atoms and influence the CB [35]. For cubic oxide Pb (Zr, Ti) O_3, the VB maximum is largely a mixture of O 2p and Pb 6s states. The CB minimum for $PbTiO_3$ is a Ti 3d

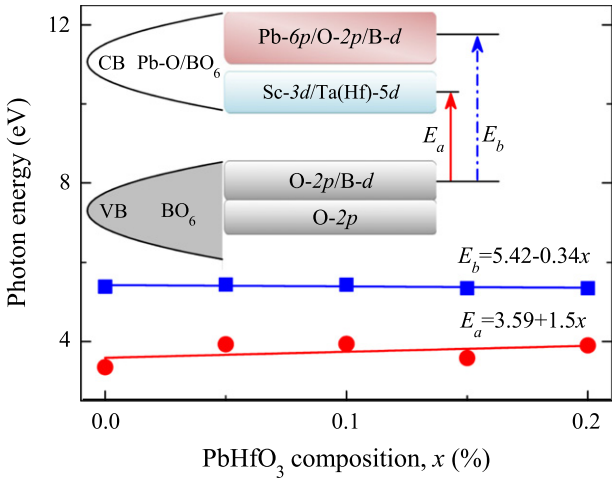

Fig. 5. Critical point energies E_a and E_b of PSTH ceramics as a function of $PbHfO_3$ composition. Note that solid lines are linearly fitting results; error bars are too small to be visible (see Table 2). The inset shows the schematic diagram of electronic band structures and the corresponding interband transitions E_a and E_b are marked by arrows. Here, the B-site atom means Sc, Ta and Hf for PSTH ceramics.

state, whereas it is largely an O *s* and Pb 6*p* state for $PbZrO_3$ [30]. For PMN, the VB mainly contains O 2*p*; the CB is mainly Nb 4*d* when derived near the band edge and becomes Pb 6*p* when derived at higher energy. Pb 6*p* and Nb 4*d* characteristics are also found at the bottom of O 2*p* bands. The hybridization of O 2*p* states with Nb 4*d* states also plays a role in the electronic density of states. For PMNT, MgO_6, NbO_6 and TiO_6 octahedra determine the basic energy level of the PMNT [36,37]. In the ordered double perovskites Sr_2ScTaO_6, the hybridization between Sc 3*d* and Ta-O t_{2g} was observed and both Ta^{5+} and Sc^{3+} make equivalent contributions to the CB [34]. Compared with the electronic structure of KTN, PZT and PMN, for PSTH, the BO_6 (B = Sc, Ta and Hf) octahedron governs the low-lying CB and the highest VB. The VB consists of the O 2*p* state and the hybridization between O 2*p* and B atoms *d* states and O 2*p* makes the major contribution to the VB maximum. The CB consists mainly of Sc 3*d*, Ta 5*d*, Hf 5*d* states and the hybridization between Pb 6*p* and Ta, Hf 5*d* states [33]. Note that O 2*p* electrons can interact with Pb 6*p* electrons in $PbHfO_3$, and that Pb–O bonding also affects the CB [33]. The schematic diagram of electronic band structures is depicted in the inset of Fig. 5 and interband transitions E_a and E_b are marked. It is concluded that the low-energy band gap E_a is attributed to transitions from the top of the VB (O 2*p*) to the bottom of the CB (B-site atoms *d* states). The E_b band gap may be due to transitions from the O 2*p* to Pb 6*p* state or the *p*-*d* hybridized states between Pb 6*p* and Ta and Hf 5*d* for the PSTH material.

Critical point energies E_a and E_b as a function of $PbHfO_3$ composition for PSTH ceramics are also plotted in Fig. 5. According to fitting parameters in Table 2, the band gap E_a is estimated to be 3.35 ± 0.18, 3.93 ± 0.04, 3.94 ± 0.04, 3.58 ± 0.14 and 3.9 ± 0.07 eV with increased $PbHfO_3$ composition. Correspondingly, the band gap E_b is 5.39 ± 0.01, 5.44 ± 0.01, 5.44 ± 0.02, 5.35 ± 0.02, and 5.35 ± 0.02 eV, respectively. Note that error bars are small, which indicates a reasonable fitting process. As can be seen, with increased $PbHfO_3$ composition (x), the band gap energy E_a (E_{01}) increases, while the parameter E_b (E_{02}) decreases slightly. For E_a, it is derived from O 2*p* to B-site *d* states and the *d* energy depends closely on B-site atom concentrations. Hence, B-site *d* states are slightly changed by the substitution of Hf ions, which induces the variation of E_a, and also suggests that the CB minimum is sensitive to B-site atom compositions. The increase of E_a will reduce the refractive index (as previously discussed). A similar phenomenon was also found in PMNT [32]. The decrease in E_b was explained by increased lattice constants in PSTH ceramics with compositions consistent with PZT [11,30]. Furthermore, interactions between O 2*p* and Pb 6*p* also affect the E_b band gap [33]. For the band gap E_b whose variation is small, the O 2*p* to Pb 6*p* state and the Pb 6*p* are insensitive to $PbHfO_3$ composition. Band gaps E_a and E_b of the present PST ceramic are 3.35 and 5.39 eV, respectively. For the KTN, interband transition energies are 3.55 and 5.13 eV and for the PZT57, these are 3.87 and 4.42 eV, respectively. The difference in the transition energies may be due to the effective electronegativity of the B ions in ABO_3 perovskite compounds [34]. In $AB'B''O_3$-type perovskite materials, the B′B″-site cation also has a strong effect on electronic structures [36]. Therefore, the variation of interband transition energy is attributed to a different B-site cation and order degree which indicates that the introduction of $PbHfO_3$ can obviously modify electronic band structures of the PSTH system.

4. Summary

Far-IR–UV reflectance spectra of relaxor ferroelectric (1-*x*) Pb $(Sc_{1/2}Ta_{1/2})$ O_3-*x*$PbHfO_3$ (PSTH) ceramics ($0 \leqslant x \leqslant 0.2$) have been measured at room temperature. The composition dependence of phonon mode frequencies is discussed, and suggests that the addition of $PbHfO_3$ has a distinct influence on lattice vibration. Dielectric functions from 0.006 to 6 eV were uniquely extracted by combining the generalized four-parameter damped oscillators and Tauc–Lorentz models. In particular, the interband transitions (critical point E_a, E_b) were analyzed by the dielectric function spectra and can be assigned to the transitions from O 2*p* to B (Sc, Ta, and Hf) *d* and Pb 6*p* states, respectively. These results show that the incorporation of $PbHfO_3$ has an important effect on optical properties and electronic band structures.

Acknowledgments

This work is financially sponsored in part by the Major State Basic Research Development Program of China (Grant No. 2011CB922200), the Natural Science Foundation of China (Grant Nos. 11074076, 60906046 and

61106122), the Shanghai Municipal Commission of Science and Technology Project (Grant Nos. 11520701300, 10DJ1400201 and 10SG28) and the Program for Professor of Special Appointment (Eastern Scholar) at Shanghai Institutions of Higher Learning.

References

[1] Wei Q, Wang ZJ, Li XZ, Long XF, Ye ZG. Chem Mater 2009;21:506.
[2] Chopra A, Birajdar BL, Kim Y, Vrejoiu L, Alexe M, Hesse D. Appl Phys Lett 2009;95:022907.
[3] Slodczyk A, Daniel P, Kania A. Phys Rev B 2008;77:184114.
[4] Kamba S, Berta M, Kempa M, Hlinka J, Petzelt J, Brinkman K, et al. J Appl Phys 2005;98:074103.
[5] Birajdar BI, Chopra A, Alexe M, Hesse D. Acta Mater 2011;59:4030.
[6] Reaney IM, Petzelt J, Voitsekhovskii VV, Chu F, Setter N. J Appl Phys 1994;76:2086.
[7] Brinkman K, Wang Y, Su D, Tagantsev A, Muralt P, Setter N. J Appl Phys 2007;102:044110.
[8] Yue X, Xiao D, Cao J, Yuan X, Yu G, Xiong X, et al. Ceram Int 2004;30:1905.
[9] Osbond PC, Whatmore RW. J Mater Sci 1993;28:1374.
[10] Liu W, Wang GS, Cao S, Mao CL, Cao F, Dong XL. J Am Ceram Soc 2010;93:2735.
[11] Liu W, Wang GS, Cao S, Mao CL, Dong XL. J Am Ceram Soc 2010;93:3023.
[12] Zhu JJ, Li WW, Xu GS, Jiang K, Hu ZG, Chu JH. Acta Mater 2011;59:6684.
[13] Zhang WJ, Li WW, Chen XG, Hu ZG, Liu W, Wang GS, et al. Appl Phys Lett 2011;99:041902.
[14] Zhang JJ, Zhai JW, Chou XJ, Shao J, Lu X, Yao X. Acta Mater 2009;57:4491.
[15] Spitzer WG, Miller RC, Kleinman DA, Howarth LE. Phys Rev 1962;126:1710.
[16] Bovtun V, Kamba S, Veljko S, Nuzhnyy D, Kroupa J, Savinov M, et al. Phys Rev B 2009;79:104111.
[17] Petzelt J, Buixaderas E, Pronin AV. Mater Sci Eng B 1998;55:86.
[18] Servoin JL, Luspin Y, Gervais F. Ferroelectrics 1981;37:523.
[19] Hlinka J, Petzelt J, Kamba S, Noujni D, Ostapchuk T. Phase Transit 2006;79:41.
[20] Hlinka J, Ostapchuk T, Noujni D, Kamba S, Petzelt J. Phys Rev Lett 2006;96:027601.
[21] Al-Zein A, Hehlen B, Rouquette J, Hlinka J. Phys Rev B 2008;78:134113.
[22] Hehlen B, Simon G, Hlinka J. Phys Rev B 2007;75:052104.
[23] Hlinka J, Simon E, Bogicevic C, Karolak F, Janolin PE. Phys Rev B 2011;84:092104.
[24] Zhong W, King-Smith RD, Vanderbilt D. Phys Rev Lett 1994;72:3618.
[25] Zhu M, Sun L, Li WW, Yu WL, Li YW, Hu ZG, et al. Mater Res Bull 2010;45:1654.
[26] Buixaderas E, Nuzhnyy D, Petzelt J, Jin L, Damjanovic D. Phys Rev B 2011;84:184302.
[27] Hu ZG, Ma JH, Huang ZM, Wu YN, Wang GS, Chu JH. Appl Phys Lett 2003;83:3686.
[28] Jellison GE, Modine FA. Appl Phys Lett 1996;69:371.
[29] Li WW, Zhu JJ, Xu XF, Jiang K, Hu ZG, Zhu M, et al. J Appl Phys 2011;110:013504.
[30] Lee H, Kang YS, Cho SJ, Xiao B, Morkoç, Kang TD, et al. J Appl Phys 2005;98:094108.
[31] Shen YQ, Zhou ZX. J Appl Phys 2008;103:074113.
[32] Chan KY, Tsang WS, Mak CL, Wong KH. Phys Rev B 2004;69:144111.
[33] Kitamura M, Chen H. Ferroelectrics 1998;210:13.
[34] Eng HW, Barnes PW, Auer BM, Woodward PM. J Solid State Chem 2003;175:94.
[35] Jan JC, Tsai HM, Pao CW, Chiou JW, Asokan K, Krishna Kumar KP, et al. Appl Phys Lett 2005;87:012103.
[36] Zhu JJ, Li WW, Xu GS, Jiang K, Hu ZG, Zhu M, et al. Appl Phys Lett 2011;98:091913.
[37] Suewattana M, Singh DJ. Phys Rev B 2006;73:224105.